Hypersonic Rugate Filters Based On Porous Silicon

L. Thomas, G.N Aliev, and P. A. Snow
Department of Physics, University of Bath, Bath BA2 7AY, United Kingdom

Periodic solid state structures exhibit transmission stopbands for waves of certain frequencies. We demonstrate porous silicon based rugate filters with 40dB rejection first-order stopbands for longitudinal acoustic waves at hypersonic frequencies and the predicted suppression of higher order bands.

Twenty years of extensive work on porous silicon (pSi), following the observation of its efficient room temperature luminescence in 1990,[1] has demonstrated the utility and adaptability of pSi as a functional material. PSi layers are produced using anodic electrochemical etching of doped silicon wafers with the etching current controlling the porosity, defined as the ratio of the void volume to the total volume of the silicon film. The doping and crystallographic direction of the wafer cut determines the pore morphology produced during etching.[2] The spatial porosity profile is determined by current modulation with time as the etch-front progresses and this also corresponds to a refractive index profile which can be used to produce optical devices. Examples include Bragg mirrors, optical filters, microcavities and devices for sensing.[3,4] Recent sensing work has used optical rugate filters, employing a sine-wave index modulation with the same fundamental frequency as the equivalent quarter-wave stack of Bragg mirrors but which give only one strong reflectivity band with reduced higher harmonics.[5]

The realization of apodized pSi optical rugate filters,[6,7] with high reflectivity and narrow bandwidth demonstrates the suitability of pSi for a variety of precision engineering applications. A theoretical study of pSi for acoustic Bragg mirrors and rugate filters has previously shown its potential for acoustic devices.[8] Recently the tunability of the physical properties of silicon with porosity has been used for hypersonic acoustic structures.[9,10] This relies on the calibration of the acoustic impedance by measuring the wave velocities as a function of porosity.[11]

The versatile nature of pSi allows the acoustic impedance of layers to be easily manipulated as a function of the porosity. The acoustic impedance profile determines the response of the multilayered device. Optimized "balanced" Bragg mirrors consist of a periodic stack of layers each of a quarter of the wavelength of the fundamental stopband. An acoustic rugate filter is periodic but with a sinusoidal modulation in its impedance-depth profile and produces one reflectivity peak per sine component of the profile.

In this letter, we present experimental and theoretical results of hypersonic rugate filters etched in pSi, with their performance compared to that of a Bragg mirror. This shows the benefits of using a continuous acoustic impedance profile. A smoothly varying acoustic impedance profile has not previously been demonstrated with pSi and few investigations have been made into such systems.[12]

At normal incidence, the Bragg frequencies, f_B, of the stopbands of an acoustic filter can be described by equation (1)[10] where M is the stopband order number, ρ_1 and ρ_2 are the mass densities of the different repeating AB layers, d_1 and d_2 are the physical thicknesses, and Z_1 and Z_2 are the characteristic acoustic impedances of the layers given by the product ρV where V is the velocity of the longitudinal acoustic wave through a layer of a specific porosity. For a balanced mirror, the bandwidth Δf can be described by equation (2) and the Bragg transmissivity T_B of the multilayered stack described by equation (3) where N is the number of repeats of the AB layer pairs.

$$f_B = \frac{M}{2}\left(\frac{\rho_1 d_1}{Z_1} + \frac{\rho_2 d_2}{Z_2}\right)^{-1} \qquad M = 1,2,3\ldots, \qquad (1)$$

$$\Delta f = \frac{4}{\pi} f_B \sin^{-1}\left(\frac{Z_2 - Z_1}{Z_2 + Z_1}\right) \qquad (2)$$

$$T_B = 4\left(\frac{Z_1}{Z_2}\right)^{2N} \Bigg/ \left(\left(\frac{Z_1}{Z_2}\right)^{2N} + 1\right)^2 \qquad (3)$$

The mass density ρ is a function of the porosity and is described by $\rho = \rho_0(1-p)$ where $\rho_0 = 2.329$ g cm^{-3} is the density of silicon and p is the porosity. Longitudinal waves are excited along the (100) crystallographic direction.[13] The acoustic velocity dependence on porosity is given empirically by $V = V_0(1-p)^k$ where $V_0 = 8.436$ km s^{-1} is the longitudinal acoustic velocity in silicon in the (100) crystallographic direction and $k = 0.595$ for these samples[11].

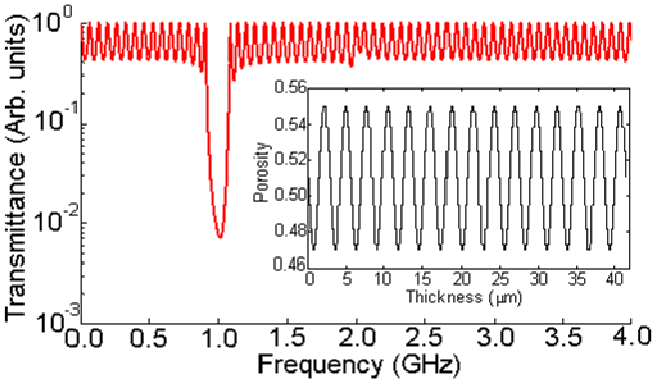

FIG. 1. Simulation of transmission through pSi acoustic rugate filter with stepped porosity profile shown in inset with p_{high}=0.55 p_{low}=0.47, half-cycle thicknesses of d_1=1.31 μm d_2=1.44 μm and N=15 repeats based on smoothing a quarter-wave Bragg mirror.

The transmissivity of dielectric structures using a continuously varying refractive index have been studied and the spectral response of rugate filters has been modeled using coupled-wave theory.[14,15] The simulated acoustic data shown in figure 1 was modeled using the transfer matrix method as described in previous publications[16]. The effect of having a continuous impedance profile has been investigated by taking a Bragg mirror design and smoothing the square wave impedance profile. A single dominant stopband is observed due to the half-period sinewave excursions from the average impedance. The profile has alternating spatial half-periods of 1.31 μm and 1.44 μm which would give quarter-wavelength layers in a Bragg mirror using porosities of 0.55 and 0.47.

Mesoporous pSi multilayered structures were etched from single-side polished boron-doped crystalline Si wafers with a resistivity of 1-5 mΩ cm. Room temperature anodization was performed using 48 wt % aqueous HF mixed with ethanol in 1:1 ratio. Etching parameters for all samples are shown in Table 1.

For the rugate structures, samples 3 and 4, the smooth variation of the porosity-depth profile was controlled using the current densities, as shown in figure 2(a). To fabricate pSi Bragg mirrors, samples 1 and 2, the etch current was alternated between a maximum and minimum value to create AB pairs of layers. An electron micrograph of a rugate filter (sample 4) is shown in figure 2(b). The layered structure seen is the effect of 30 etch cycles as shown in fig 2(a). Etch stops of three seconds were found to be sufficient to prevent HF depletion and hence drift of average porosity with depth.[17]

In this case each half-sinusoidal cycle (corresponding to layer A or B) was split into 8 more individual sub-layers where the physical thickness of the overall layer A or B was controlled by the etch time in the 8 sub-layers.[6] Modeling showed this to be a sufficient number of steps in current density to fabricate a sinusoidal variation in impedance such that a rugate mirror response equivalent to a sine profile was achieved.

TABLE. I. Etch parameters used to fabricate pSi multilayered samples with resulting porosities and thicknesses (N= No. of etch cycles).

Sample	I_1 (mA)	I_2 (mA)	P_{low}	P_{high}	d_1 (μm)	d_2 (μm)	N
I	500	600	0.61	0.71	2.17	1.05	15
II	470	690	0.59	0.73	1.55	1.84	15
III	470	690	0.58	0.72	1.59	2.11	15
IV	484	684	0.62	0.71	1.21	1.21	30

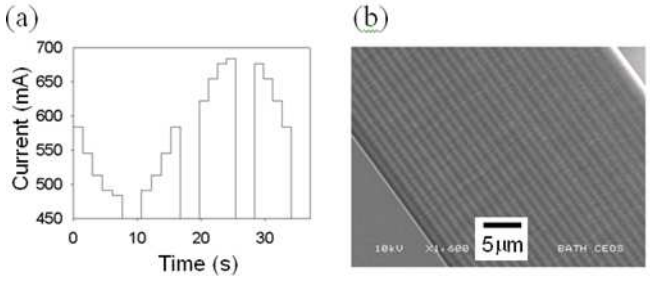

FIG. 2. (a) Current-time etch profile of one cycle used for sample 4. (b) SEM image of pSi rugate filter sample 4.

The multilayered rugate structures have been characterized by scanning electron microscope (SEM) imaging as shown in figure 3(a) and 3(c) to determine layer thicknesses. The contrast changes of the micrograph images due to electron density of the varying porosity material within the multilayers were used to extract a contrast profile analogous to the porosity profile as shown in figure 3(b) and 3(d). The effect of etch stops in the cycle are evident from the small peaks in the SEM contrast profile. The surface of the wafer has some charging with respect to the conductive substrate which has introduced an artificial gradient to the overall contrast profile.

Samples were placed between two silicon pillar ultrasonic transducers (160 μm x 160 μm x 500 μm) with a fundamental operating bandwidth centered at ~1 GHz.[10] High power driving of the transducers allowed higher order longitudinal modes of the transducer to be excited and measured, enabling excitation of frequencies up to 3 GHz. Gallium-indium eutectic which does not appear to infiltrate the pores due to surface tension, was used as the coupling liquid to couple longitudinal waves into the pSi at normal incidence. Acoustic transmission measurements were performed using a vector network analyzer (VNA). The transmittance results presented below have been normalized to the transducer frequency response

measured with no Si sample but only eutectic between the transducers.

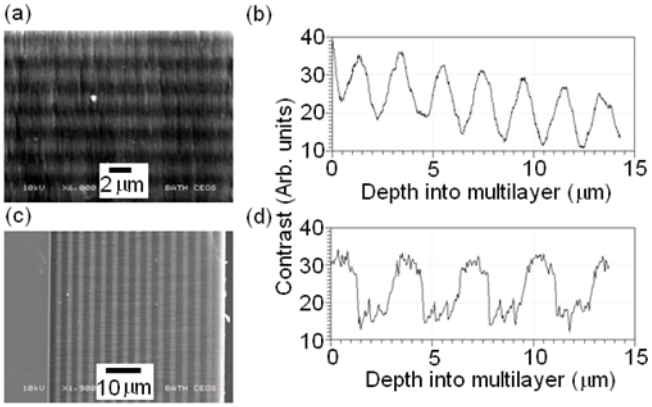

FIG. 3. (a) SEM image of a pSi rugate filter etched with 32 sub-layers and (c) pSi Bragg mirror sample 2. (b) SEM contrast profile of the pSi rugate filter of (a) showing filter period thickness of 2.14 μm and (d) sample 2.

Samples 2 and 3 have the same nominal maximum and minimum porosities and number of etch cycles to compare the properties of a Bragg and rugate porosity profile. The expectation is that the fundamental stop band bandwidth of the rugate filter is π/4 (78%) that of the bandwidth of the Bragg mirror[18]. This is the case for the simulated data of figure 4(a). However the measured rugate filter bandwidth of figure 4(b) is 68% that of the Bragg mirror equivalent bandwidth. Due to the transmission measurement being limited by the noise floor of the VNA and transducers, the depth of the measured stop bands were limited whilst the simulation is lossless. The transmittance of samples 2 and 3 shown in figure 4(b) have the same measured fundamental stopband depth of 40 dB, with sample 2 having a fundamental Bragg frequency of 0.64 GHz and bandwidth of 0.25 GHz. The higher order harmonic of the rugate filter, sample 3, is heavily suppressed.

In figure 4(c), it can be seen that the unbalanced pSi Bragg mirror (sample 1) has four measurable stop bands with the fundamental mode located at 0.7 GHz with bandwidth of 0.17 GHz. Higher order modes are located at higher frequencies with $M = 2$ at 1.4 GHz, $M = 3$ at 2.1 GHz and $M = 4$ at 2.8 GHz. In figure 4(d) the rugate filter, sample 4, displays only the fundamental stopband at 0.95 GHz with bandwidth of 0.2 GHz and stopband depth of 40 dB.

We have demonstrated that by controlling the etch parameters during electrochemical etching of pSi, it is possible to fabricate all-Si acoustic rugate filters, which use a smooth acoustic impedance profile. As expected from their optical analogs, the acoustic rugate filters show suppression of higher order stopbands. In future work it will be possible to create other acoustic devices with smoothly varying acoustic impedance profiles to be used, for example, as anti-reflection coatings for transducers, index-matching layers or filters that have apodization functions. It is also possible to create a superposition of filters suitable for a wide range of frequencies.

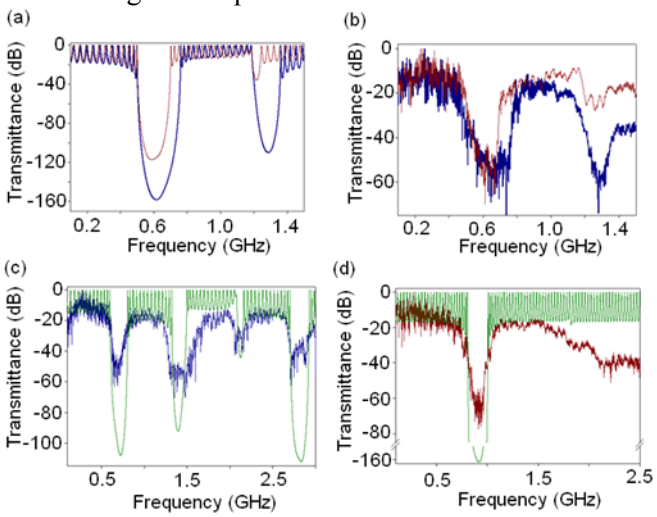

FIG. 4. (Color online) Measured and modeled differences between Bragg and rugate filters. (a) Simulated data for sample 2 (thick line) and sample 3 (thin line). (b) acoustic transmission measurements for unbalanced pSi Bragg mirror sample 2 (thick line) and pSi rugate filter sample 3 (thin line). For (c) and (d): thick curves are acoustic transmission measurements for (c) sample 1 and (d) sample 4. The thin curves are simulated response.

This work was funded by EPSRC (Project No. EP/C010469/1).

[1] L. T. Canham, Appl. Phys. Lett. **57** (10) 1046 (1990)
[2] Leigh Canham, *Properties of Porous Silicon*, (INSPEC, London, 1997)
[3] P. A. Snow, E. K. Squire, P. St. J. Russell and L. T. Canham, J. Appl. Phys. **86** 1781 (1999)
[4] V. Torres-Costa and R. J. Palmer J. Mater. Sci. **45** 2823 (2010)
[5] F. Cunin, T. A. Schmedake, J. R. Link, Y. Y. Li, J. Koh, S. N. Bhatia, and M. J. Sailor, Nature Mat. **1** 39 (2002)
[6] E. Lorenzo, C. J. Oton, N. E. Capuj, M. Ghulinyan, D. Navarro-Urrios, Z. Gaburro and L. Pavesi, Appl. Opt. **44** 5415 (2005)
[7] S. Ilyas, T. Böcking, K. Kilian, P. J. Reece, J. Gooding, K. Gaus, M. Gal, Opt. Mat. **29** 619 (2007)
[8] A. Reinhardt and P. A. Snow, Phys. Stat. Sol. **204** 1528 (2007)
[9] L. C. Parsons and G. T. Andrews, Appl. Phys. Lett. **95** 241909 (2009)
[10] G. N. Aliev, B. Goller, D. Kovalev and P. A. Snow, Appl. Phys. Lett. **96** 124101 (2010)
[11] G. N. Aliev, B. Goller, D. Kovalev and P. A. Snow, Phys. Stat. Sol. C **6** 1670 (2009)
[12] L. Guillon and X. Lurton, Acta. Acust. Acust. **88** 611 (2002)
[13] B. A. Auld, *Acoustic Fields and Waves in Solids- Volume 1*, 2nd ed. (Krieger, Malabar-Florida, 1990)
[14] W. H. Southwell, J. Opt. Soc. Am. A **5** 1558 (1988)
[15] B. G. Bovard, Appl. Opt. **32** 5427 (1993)
[16] C. L. Mitsas and D. I. Siapkas, Appl. Opt. **34** 1678 (1995)
[17] M. Thönissen, M. G. Berger, S. Billat, R. Arens-Fischer, M. Krüger, H. Lüth, W. Theiss, S. Hillbrich, P. Grosse, G. Lerondel, U. Frotscher, Thin Solid Films **297** 92-96 (1997)
[18] W. H. Southwell, Appl. Opt. **36** 314 (1997)